Numerical experiments on the gas flow between eccentric rotating cylinders

L. M. de Socio[a] and L. Marino[b],*

[a] *Dipartimento di Meccanica e Aeronautica, Via Eudossiana 18, Roma, Italy*
[b] *Dipartimento di Metodi e Modelli Matematici per le Scienze Applicate, Via A. Scarpa 16, Roma, Italy*

SUMMARY

A numerical experiment was carried out on the gas flow field between two eccentric cylinders, one of which is rotating. Attention was paid to the presence of separated recirculating regions from the continuum to the rarefied regimes. The direct simulations were performed by means of a Monte Carlo (DSMC) method and bi-polar co-ordinates were adopted. The calculations were relative to isothermal walls at the same temperature. Streamlines and velocity profiles were evaluated as functions of the Knudsen number, of the Mach number and of the geometric parameters. The gas considered was argon. Copyright © 2000 John Wiley & Sons, Ltd.

KEY WORDS: eccentric rotating cylinders; rarefied gas flow; Knudsen number effect

1. INTRODUCTION

The gas flow field between rotating cylinders has been investigated for a long time now, both experimentally and from the analytical and numerical points of view. This is a consequence of the important applications and of the physico-mathematical interest for this kind of flow. The majority of existing results concern the axisymmetric plane geometry, for which exact analytical solutions are known in a wide range of the pertinent dimensionless characteristic numbers from the continuum regime to the free molecular flow.

The eccentric case, which is much more complex than the one-dimensional axisymmetric geometry, has been analytically dealt with in the continuum regime by following substantially approximate formulations. To the authors' knowledge, the only closed form solution is the one relative to the Stokes linear flow model, which was firstly presented in Reference [1] and a little later in References [2,3]. Numerical solutions are practically the only available solutions to the problem; however, even in this case, the continuum regime is the flow situation that is usually referred to in literature. In fact the number of governing dimensionless products is relatively

---

* Correspondence to: Dipartimento di Metodi e Modelli Matematici per le Scienze Applicate, Universitá 'La Sapienza', Via A. Scarpa 16, I-00161 Roma, Italy.

high and a full exploration of the influence of each of them on the fluid field is still an open research area. Finite elements and non-linear boundary integrals are the main tools that have been adopted for treating this eccentric geometry [4–6], when only one of the walls is rotating. Further numerical solutions have been obtained by a Galerkin expansion procedure in Reference [5], where both walls are considered to rotate. We also cite here the attempts to find approximate analytical solutions by means of power series expansions in terms of either an eccentricity parameter [7] or the Reynolds number [8]. In the latter article, a similar linearization approach as that reported in Reference [3] is shown to be incorrect.

In this paper, the motion characteristics between the walls of two eccentric isothermal cylinders, one of which—in general the external one—is rotating, are dealt with. A very wide range of Knudsen numbers is considered ($10^{-3} \sim 10$) so that the flow regimes from the continuum to the free molecular flow are investigated. In particular, the possible presence of a recirculation region is dealt with by taking the effects of eccentricity, gas rarefaction and rotational speed of the wall into account.

The investigation was carried out by a direct simulation method in order to perform numerical experiments. For the purpose of comparison, some results were also obtained in situations where either analytical or numerical solutions were already available. The numerical code was based on a Monte Carlo procedure and bi-polar co-ordinates were taken as reference axes. This choice greatly simplified the representation of the borders of the computational domain, although in so doing some complications were introduced when calculating the rectilinear trajectories of the particles.

Figure 1 is a sketch of the considered geometry where the bi-polar axes, in the reference plane, are represented by two families of circles at constant ξ and η values. Let $\delta R = R_2 - R_1$ be the average width of the gap between the cylinders of radii R_1 and R_2, which correspond to the lines ξ_1 and ξ_2 respectively, and let d be the distance between the centres of the cylinders. Then the ratio $r = R_1/R_2$, the ratio of specific heats γ and the ratio Θ of the temperature of the
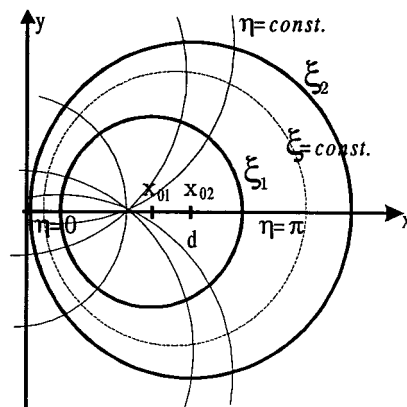
Figure 1. Geometry.

internal wall T_1 to the temperature of the external one T_2 correspond to a first group of dimensionless products, which will be assumed constant in the present analysis unless otherwise specified. In particular, one has $r = 0.45$, $\gamma = 1.667$ is that of argon and $\Theta = 1$. Furthermore, let Ω be the angular speed of the external cylinder, $V_2 = R_2\Omega$ its tangential velocity and let c_2 be the speed of sound of the gas at T_2. Then, the Mach number of the rotating wall $Ma_2 = \Omega R_2/c_2$, the eccentricity $e = d/\delta R$ and the reference Knudsen number Kn_0 form a second group of dimensionless products, the influence of which on the flow field will be studied. Here, $Kn_0 = \lambda_0/\delta R$, where λ_0 is the gas mean free path at the average mass density ρ_0. We will consider sometimes the reference Reynolds number $Re_0 = \rho_0\Omega R_2^2/\mu_0$, for which the relation $Re_0 = k_1 Ma_2/Kn_0$, where $k_1 = 2.91$ for argon, holds.

The reference density ρ_0 and viscosity μ_0 correspond to the equilibrium situation where both the walls are at rest.

Throughout the paper, dimensionless quantities will be adopted, the reference length and velocity being δR and V_2 respectively. Also T_2 is the reference temperature.

2. THE DIRECT SIMULATION

Different methods have been proposed for the direct simulation of the molecular dynamics of the fluids. In particular, when dealing with gases, the time history of ensembles of particles is calculated following the dynamics of each representative particle through its collisions against other particles and boundaries. The motion equations are solved under the proper assumptions concerning the characteristics of the boundaries, of the molecules and of their random encounters. The initial velocity distribution among the particles is randomly assigned and the macroscopic variables of the thermo-fluid dynamic state are statistically evaluated at the end of the solution procedure.

Our direct simulation was carried out by means of a Monte Carlo (DSMC) procedure, which is based on the method presented by Bird in his well known book [9].

Care was paid to the choice of the grid, to the proper determination of the volume elements in the bi-polar co-ordinate system and to the calculation of the particle dynamics, where all the properties of the argon molecules were taken from Reference [9]. The boundaries are assumed as completely diffusive walls that re-emit the impinging molecules according to a Maxwellian velocity distribution function.

The elemental area in the plane (ξ, η) is given by

$$\Delta A(\xi, \eta) = \int \frac{1}{(\cosh \xi + \cos \eta)^2} \, \mathrm{d}\xi \, \mathrm{d}\eta$$

and Figure 2(a) and (b) provides the distribution of ΔA as a function of ξ for the three values $\eta_1 = 0$, $\eta_2 = \pi/2$ and $\eta_3 = \pi$. For convenience of interpretation in these figures and in what follows, the transverse variable $\bar{\xi} = (\xi - \xi_2)/(\xi_1 - \xi_2)$ has been introduced. Constant values of $\Delta\xi$ and $\Delta\eta$ do not correspond to a constant ΔA distribution in the domain.

Figure 2(a) and (b) shows that, for an assigned $\Delta\eta$, a proper choice of $\Delta\xi$ as a function of e provides a reasonable ΔA distribution, which privileges those regions where sizeably greater
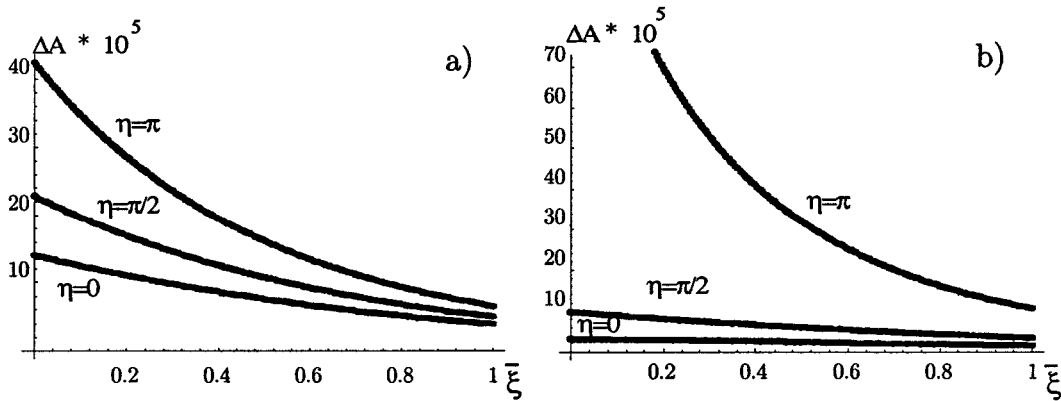
Figure 2. Area distributions for $\Delta \eta = 6.28 \times 10^{-2}$: (a) $\Delta \xi = 7.88 \times 10^{-3}$, $e = 0.2$; (b) $\Delta \xi = 6.36 \times 10^{-3}$, $e = 0.6$.

gradients of flow parameters are expected and greater accuracy is desirable. In particular, note the role played by the eccentricity on the ΔA distribution. A finer grid is adjacent to the internal wall, where separation effects are likely to be present. According to Bird's simulation model, the average dimensionless velocity components different from zero are v_ξ and v_η, but the random particle velocity has all its three components (q_ξ, q_η, q_ζ) in a dimensionless volume $\Delta \mathcal{V} = \Delta A \cdot \Delta \zeta$, where $\Delta \zeta$ is the unit length in the direction normal to the plane (ξ, η).

Since the trajectory of a particle after colliding either with a wall or with another particle is a straight line, the transformation (A.1) in Appendix A was used, with x and y Cartesian co-ordinates as in Figure 1, and the final position was calculated via the inverse transformation (A.2) including—eventually—either the crossing of the borders of ΔA or the re-emission from the cylindrical boundaries.

The evaluation of the convergence characteristics of the solution procedure was obtained by a criterion based on the values of the fluid dynamic state parameters in a control cell. When the norm of the differences of these values between two calculation steps, and after an assigned number of steps, fell below an assigned criterion ϵ, the computations were assumed to have converged. In particular, the reference cell for the convergence test was chosen at $\eta = \pi/2$ and at the middle of the gap, $\bar{\xi} = 0.5$. Different choices led to practically the same results. The criterion for the tangential velocity $|\Delta v_r/v_r|$ in the reference cell was $\epsilon = 10^{-3}$ and for the number density $|\Delta n_r/n_r|$, $\epsilon = 10^{-4}$. The influence of the grid dimensions and of the number of representative particles on satisfying the convergence criterion was explored in the range of dimensionless products to be considered.

An example of the convergence characteristics of the code is reported in Figure 3(a) and (b), which are relative to the case $e = 0.6$, $Kn_0 = 0.1$, $r = 0.45$ and $Ma_2 = 0.5$. The maximum value of the number of representative particles was 600 000 with 200×200 cells.

The majority of the cases reported in this paper were run with a grid of 200×200 elements and 400 000 representative particles on an ALPHA EV56-21164A processor and an average run required about 48 h.
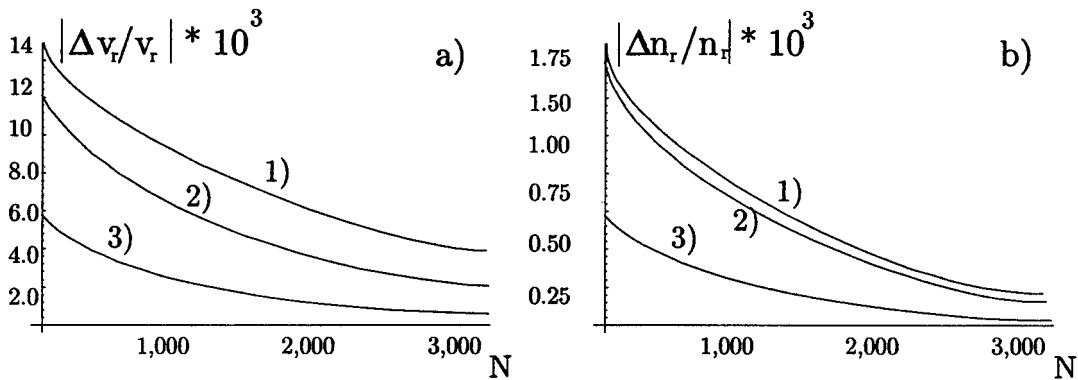
Figure 3. Convergence of the tangential velocity (a), and number density (b) as function of steps N: 1) 100×100 cells, $100\,000$ particles; 2) 200×200 cells, $100\,000$ particles; 3) 200×200 cells, $600\,000$ particles.

The analytical (either exact or approximate) solutions that exist in the pertinent literature are relative to the case of an incompressible continuum medium. In these circumstances, the dominant parameter is Re_0 as both Ma_2 and Kn_0 are, as a consequence, assumed equal to zero. Then, a direct comparison with the results of our simulation method would be—of course —impossible. However, we solved a few cases where it seemed reasonable to judge the accuracy of the DSMC in predicting the main flow field characteristics in the framework of exact either analytical or numerical solutions.

In order to evaluate the reliability of the direct simulation in obtaining accurate results, we compared our DSMC results with the exact analytical results of Farris [2] for the Stokes flow. The linear Stokes flow equation corresponds to the Navier–Stokes incompressible continuum for a Reynolds number that is vanishingly small and is often taken as a test problem for numerical procedures [10–12].

When running a DSMC code, which by necessity deals with compressible gases, a meaningful small value of $Re \propto Ma/Kn$ can be treated for a Kn value not too small to simulate a continuum gas and a Mach number value not too high (for incompressibility). In the case of $e = 0.4$, $r = 0.7$, we chose $Kn_0 = 0.01$ and $Ma_2 = 0.5$ in our simulation and compared the results with those in Reference [2].

As one can realise by observing Figure 4, the comparisons of the tangential velocity profiles calculated at three different locations, $\eta = 0$, $\pi/2$ and π, are really good.

A second comparison is relative to the case $Re_0 = 300$, $e = 0.5$, $Kn_0 = 0.01$, which had been solved by applying a boundary element method to the Navier–Stokes equation in Reference [5]. Note that in this case, the rotating wall is the internal one, with $Ma_1 = 0.5$. In Figure 5(a) and (b) we show the velocity profiles in two sections, corresponding to the wide and to the narrow gap respectively, as calculated in Reference [5] and by direct simulation. The agreement between the results obtained via the two approaches is again very good.
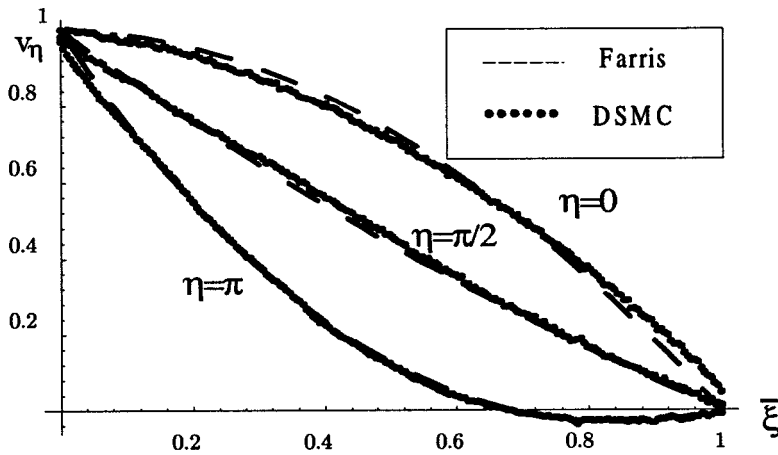
Figure 4. Tangential velocity profiles. Comparisons between the solutions of Reference [2] and the simulation results.
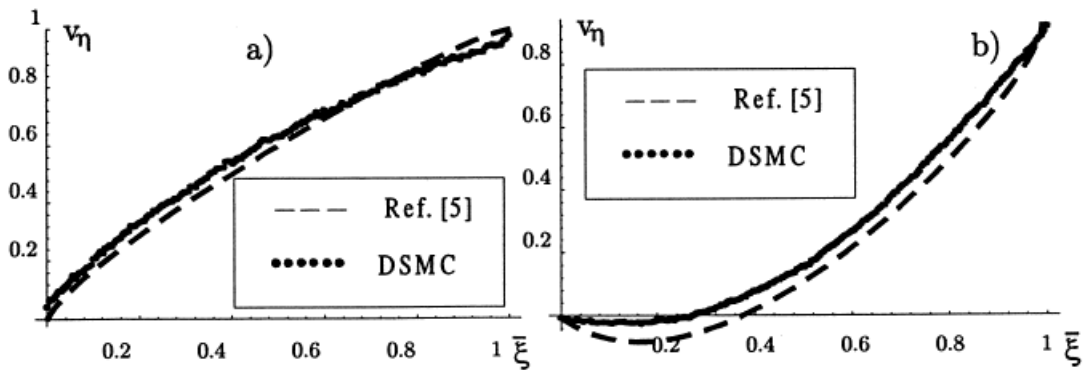
Figure 5. Tangential velocity profiles at the wide gap (a), and at the narrow gap (b). Comparisons between the solutions of Reference [5] and the simulation results.

Our last comparison is relative to the case solved by Rivlin and Ballal [8], where a couple of counter-rotating walls is considered with $Ma_2/Ma_1 = 7$, $Re_0 = 100$ and $e = 0.4$, $r = 0.3$.

The results, not reported, show a good agreement between the first-order approximate values of [8] and the DSMC calculated ones. As an example the location of the stagnation point on $\eta = 0$ is $\bar{\xi} = 0.48$ in Reference [8] and this value favourably compares with $\bar{\xi} = 0.47$ of our calculations.

At this point the code can be thought of as satisfactorily tested and the following section is dedicated to the parametric analysis of the problem.

3. ANALYSIS OF RESULTS AND CONCLUSIONS

The main goal of this section is the study of the influence of the basic parameters on the presence of a separated flow region.

As a reference we started from the analytical solution to the Stokes problem and evaluated the conditions under which a vortical region appears close to the internal wall. After setting the normal derivative of the peripheral velocity at the internal cylinder equal to zero, we obtained the condition for the zero shear stress and this expression was solved in terms of e and r (see Appendix B). Table I shows a few calculated results where e_s is the value of the eccentricity, at a given r, beyond which separation occurs

As mentioned before, the data in Table I refer to the case of a continuum flow at a very low Re_0. If we take the influence of rarefaction into account, e.g. for $e = 0.6$, $r = 0.45$, $Ma_2 = 0.5$, let us consider the three cases $Kn_0 = 10^{-3}$, 10^{-1} and 10. Figure 6(a)–(c) shows the corresponding streamline distributions, whereas Figure 7(a) and (b) compares the Farris velocity profiles with the DSMC results. An example of the velocity field is reported in Figure 8.

Understandably, the gas rarefaction delays the appearance of the separated region, which eventually disappears as one moves towards the free molecular regime. This can be better realized if one considers that the wall separation is more immediately related to the local Reynolds number $Re \cong Ma/Kn$, which, for low values of Ma_2, essentially depends upon the local Kn value. This means that moderate changes of Ma do not produce significant effects on separation. The results (not shown) obtained for $Ma_2 = 1$ are practically coincident with those for $Ma_2 = 0.5$. On the other hand, as Ma_2 increases further, a high local Kn region appears near the internal wall as a consequence of the increased centrifugal effects, and while all the other parameters are kept constant, an eventually present vortical region can progressively disappear.

Table I. Eccentricity values above which separation occurs in Stokes flow.

$r = R_1/R_2$	$\rightarrow$	0.01	0.10	0.25	0.45	0.75	0.90
e_s	$\rightarrow$	0.03	0.15	0.22	0.27	0.26	0.29
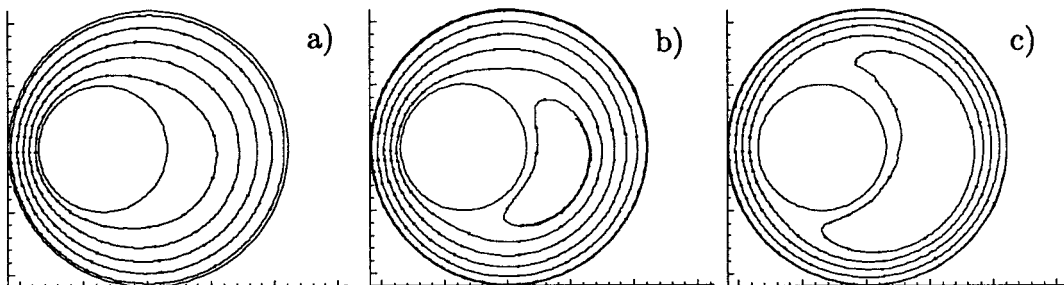
Figure 6. Streamlines that show the presence of a separated region for $e = 0.6$, $r = 0.45$, $Ma_2 = 0.5$ and $Kn_0 = 10$ (a), 0.1 (b), 0.001 (c).
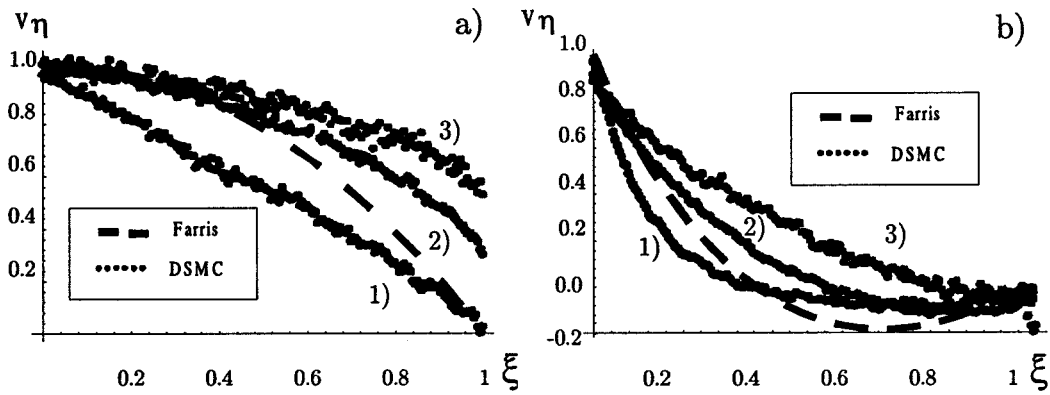
Figure 7. Tangential velocity profiles versus $\bar{\xi}$ at $\eta = 0$ (a), $\eta = \pi$ (b); 1) $Kn_0 = 0.0011$, 2) $Kn_0 = 0.1$, 3) $Kn_0 = 10$. The Farris solution is also shown.
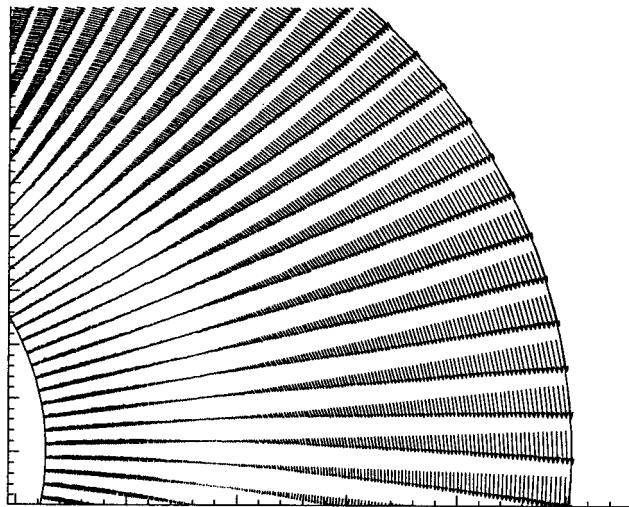
Figure 8. Close up view of the velocity vector field in the case of Figure 6(b).

When the influence of the eccentricity is finally dealt with we note that the appearance of a separated region occurs at higher values of Kn_0 as e increases. Figure 9(a) and (b) shows the changes for $Kn_0 = 0.1$ and for e increasing from 0.4 to 0.6. Note, from Table I for the Stokes model, that $e = 0.4$ is greater than 0.27 at which a separated region first appears. When the rarefaction effects increase, the velocity slip at the walls becomes greater and the presence of a separated region, induced by high values of the shear stress, disappears. If we consider the
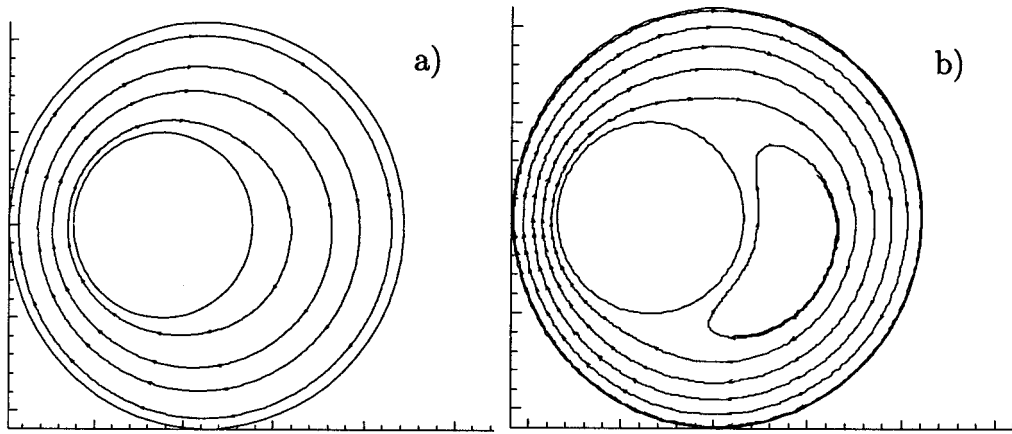
Figure 9. Influence of the eccentricity on the presence of a separated region. $Kn_0 = 0.1$; $Ma_2 = 0.5$; $r = 0.45$; $e = 0.4$ (a), 0.6 (b).

same value as before $e = 0.4$, but $Kn_0 = 0.001$, Figure 10(a) and (b) confirms the presence of separation in the continuum regime. Figure 10(b) also shows the difference between the Stokes case and that for $Kn_0 = 0.001$ as far as the velocity profiles are concerned.

Before ending this section we note that the influence of r on separation can be discussed from the data reported in Table I and the results of Figure 4, which both show that separation occurs at lower values of r, i.e. as the mean gap increases, for lower eccentricity.
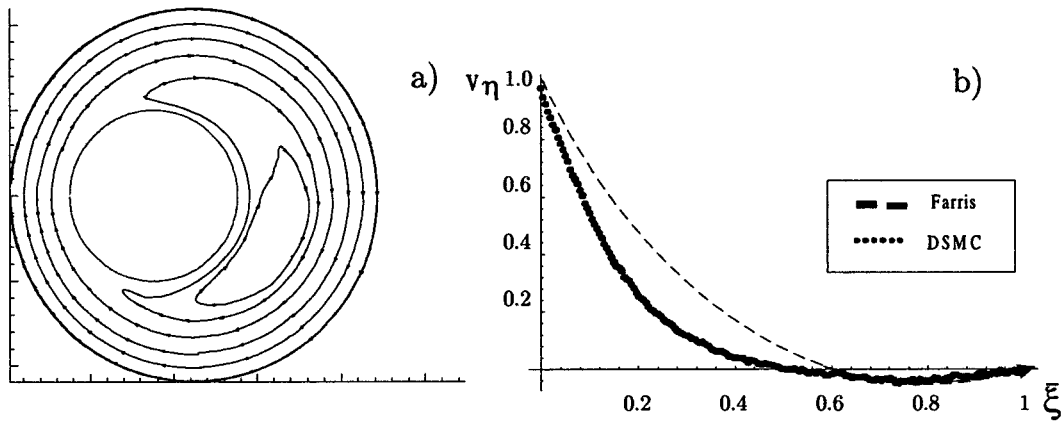
Figure 10. $Kn_0 = 0.001$, $Ma_2 = 0.5$, $r = 0.45$, $e = 0.4$; streamlines (a), tangential velocity profiles (b).

As a conclusion of the paper we observe that the direct simulation is a powerful method for obtaining accurate results in a complex fluid dynamic situation as the one where flow separation occurs. This was proved as a first step by comparison with existing reliable data in the continuum regime between rotating cylinders. Among the great number of dimensionless parameters that govern the fluid dynamic field, attention was paid to the most significant ones in the case of non-coaxial rotating cylinders, i.e. the rotating wall Mach number, the Knudsen number and the eccentricity. In particular, the noticeable influence of the gas rarefaction in suppressing the presence of a recirculating region, which is, on the other hand, favoured by an increasing eccentricity, was shown.

APPENDIX A

The equations of the transformation from Cartesian to bi-polar co-ordinates are

$$x = s\,\text{Sinh}\,\xi/\beta, \qquad y = a\,\text{Sin}\,\eta/\beta \tag{A.1}$$

where the geometric parameter a is defined as

$$a = R_2^2\{1 - (R_1^2/R_2^2)[2 - R_1^2/R_2^2] - (d^2/R_2^2)[2 - d^2/R_2^2 + 2R_1^2/R_2^2]\}^{1/2}/(2d\delta R)$$

and

$$\beta = \text{Cosh}\,\xi + \text{Cos}\,\eta$$

The inverse transformations are

$$\eta = \text{ArcTan}[2ay/(a^2 - x^2 + y^2)]$$

$$\xi = \text{ArcTanh}[2ax/(a^2 + x^2 + y^2)] \tag{A.2}$$

The circle $\xi = $ constant is represented by

$$x^2 + y^2 - \frac{2a}{\text{Tanh}\,\xi}x + a^2 = 0$$

while the $\eta = $ constant is

$$x^2 + y^2 - \frac{2a}{\text{Tan}\,\eta}x - a^2 = 0$$

This means that the loci $\xi = $ constant and $\eta = $ constant are circles with centres and radii

$$
\begin{cases}
x_0 = a/\text{Tanh } \xi \\
y_0 = 0 \\
R_\xi = |a/\text{Sinh } \xi|
\end{cases}
$$

and

$$
\begin{cases}
x_0 = 0 \\
y_0 = a/\text{Tan } \eta \\
R_\eta = |a/\text{Sin } \eta|
\end{cases}
$$

respectively. The two circles with radii R_1 and R_2 correspond to

$$\xi_1 = \text{ArcSinh}(a/R_1), \qquad \xi_2 = \text{ArcSinh}(a/R_2)$$

with centres

$$x_{01} = a/\text{Tanh } \xi_1, \qquad x_{02} = a/\text{Tanh } \xi_2$$

APPENDIX B

For the Stokes problem, the streamline function Ψ is [2]

$$\Psi = f/\beta + h$$

where

$$f = E \text{ Sinh } \xi + F \text{ Cosh } \xi + G\xi \text{ Sinh } \xi + H\xi \text{ Cosh } \xi - 1/2(A \text{ Sinh } \xi + B \text{ Cosh } \xi)$$

$$h = A \text{ Sinh } 2\xi + B \text{ Cosh } 2\xi + C\xi$$

and with A, B, C, E, F, G and H constants that depend on the boundary conditions and on the geometry of the problem, in particular e and r. The zero shear stress can be obtained from the condition

$$\left.\frac{\partial v_n}{\partial \xi}\right|_{\xi = \xi_1, \ \eta = 0} = \text{Cosh } \xi_1 - f''(\xi_1)/h''(\xi_1) = 0$$

REFERENCES

1. Wannier GH. A contribution to the hydrodynamics of lubrication. *Quarterly Journal of Applied Mathematics* 1950; **8**: 1–32.
2. Farris GJ. Flow in a journal bearing. MS thesis, North Western University, Evanston, IL (as reported in Enffilich R, Slattery CJ. Evaluation of power-model lubricants in an infinite journal bearing. *I&EC Fundamentals* 1968; **7**: 239–240), 1962.
3. Kamal MM. Separation in the flow between eccentric rotating cylinders. *Journal of Basic Engineering*, *ASME* 1966; **88**: 717–724.
4. Araujo JHC, Ruas V, Vargas AS. Finite element solution of flow between eccentric cylinders with viscous dissipation. *International Journal of Numerical Methods in Fluids* 1990; **11**: 849–865.
5. Ramesh PS, Lean MH. A boundary integral equation method for Navier–Stokes equations. Application to flow in annulus of eccentric cylinders. *International Journal of Numerical Methods in Fluids* 1991; **13**: 355–369.
6. San Anders A, Szeri AZ. Flow between eccentric rotating cylinders. *Journal of Applied Mechanics*, *ASME* 1984; **51**: 869–878.
7. Wood WW. The asymptotic expansions at large Reynolds numbers for steady motion between non-coaxial rotating cylinders. *Journal of Fluid Mechanics* 1957; **8**: 159–175.
8. Ballal BY, Rivlin RS. Flow of a Newtonian fluid between eccentric rotating cylinders: inertial effects. *Archive of Rational Mechanics and Analysis* 1977; **62**: 237–294.
9. Bird GA. *Molecular Gas Dynamics and the Direct Simulation of Gas Flows*. Clarendon Press: Oxford, 1994.
10. Gresho PM, Lee RL, Sani RL, Maslanik MK, Eaton BE. The consistent Galerkin FEM for computing derived boundary quantities in thermal and/or fluids problems. *International Journal of Numerical Methods in Fluids* 1987; **7**: 371–394.
11. Sani RL, Gresho PM, Lee RL, Griffiths D, Engelman. MS. The cause and cure (?) of the spurious pressure generated by certain FEM solutions of the incompressible Navier–Stokes equations. *International Journal of Numerical Methods in Fluids* 1981; **1**: 17–43.
12. Maslanik MK, Sani RL, Gresho RM. An isoparametric finite-element Stokes flow test problem. *Communications in Applied Numerical Methods* 1990; **6**: 429–436.